RESEARCH Open Access

# EBV Reactivation-associated gene signature predicts poor prognosis in nasopharyngeal carcinoma

(2025) 23:616



Qingshuang Luo<sup>1,2†</sup>, Jingyi Long<sup>1,2†</sup>, Longtai Hu<sup>1,2†</sup>, Moyed Alsaadawe<sup>1,2</sup>, Oluwasijibomi Damola Faleti<sup>1,2,3</sup> and Xiaoming Lyu<sup>1,2,4\*</sup>

#### **Abstract**

**Background** Epstein-Barr virus (EBV) reactivation is closely associated with poor prognosis in nasopharyngeal carcinoma (NPC). However, the molecular mechanisms underlying EBV reactivation in NPC progression remain unclear. This study aimed to identify key genes and pathways involved in EBV reactivation using an integrated multiomics approach.

**Methods** An in vitro EBV reactivation model was established to investigate molecular changes associated with viral reactivation. Transcriptomic (RNA-seq) and proteomic (LC-MS/MS) analyses were performed to identify differentially expressed genes. Functional enrichment, protein-protein interaction network analysis, and survival analysis were conducted to elucidate the biological significance of key genes. RNA-seq data from NPC patients (GSE102349) were analyzed to assess the association between EBV reactivation (BZLF1 expression) and clinical outcomes.

**Results** A ten-gene signature (PLAUR, SBSN, LAMC2, CDC42EP1, F3, S100A, CYP24A1, KRT6B, PTGS2, and NQO1) was identified as significantly associated with EBV reactivation. These genes are involved in epithelial-mesenchymal transition (EMT), metabolic reprogramming, and hypoxia response. Pathway analysis highlighted their roles in complement and coagulation cascades, laminin interactions, keratin complex formation, and metabolic regulation, all of which contribute to EMT. Additionally, analysis of NPC patient data (GSE102349) revealed a correlation between BZLF1 expression and poor prognosis.

**Conclusions** This study identifies a novel prognostic gene signature associated with EBV reactivation in NPC through integrated multi-omics analyses, which provided insights into the molecular mechanisms of NPC progression. These findings suggest potential diagnostic and therapeutic targets for improving NPC.

Keywords EBV reactivation, Nasopharyngeal carcinoma, Multi-omics analysis, Prognostic biomarkers



© The Author(s) 2025. **Open Access** This article is licensed under a Creative Commons Attribution-NonCommercial-NoDerivatives 4.0 International License, which permits any non-commercial use, sharing, distribution and reproduction in any medium or format, as long as you give appropriate credit to the original author(s) and the source, provide a link to the Creative Commons licence, and indicate if you modified the licensed material. You do not have permission under this licence to share adapted material derived from this article or parts of it. The images or other third party material in this article are included in the article's Creative Commons licence, unless indicated otherwise in a credit line to the material. If material is not included in the article's Creative Commons licence and your intended use is not permitted by statutory regulation or exceeds the permitted use, you will need to obtain permission directly from the copyright holder. To view a copy of this licence, visit http://creativecommons.org/licenses/by-nc-nd/4.0/.

<sup>&</sup>lt;sup>†</sup>Qingshuang Luo, Jingyi Long and Longtai Hu contributed equally to this work.

<sup>\*</sup>Correspondence: Xiaoming Lyu xiaomlyu@smu.edu.cn

<sup>&</sup>lt;sup>1</sup>Department of Laboratory Medicine, The Third Affiliated Hospital of Southern Medical University, Guangzhou 510630, China

<sup>&</sup>lt;sup>2</sup>The Third School of Clinical Medicine, Southern Medical University, Guangzhou 510630, China

<sup>&</sup>lt;sup>3</sup>Department of Applied Biology and Chemical Technology, The Hong Kong Polytechnic University, HKSAR 999000, China

<sup>&</sup>lt;sup>4</sup>Department of Laboratory Medicine, The Third School of Clinical Medicine, The Third Affiliated Hospital, Southern Medical University, Guangzhou 510630, China

#### Introduction

Nasopharyngeal carcinoma (NPC) is a highly aggressive head and neck malignancy that arises from the epithelial lining of the nasopharynx and displays unique epidemiological and etiological features [1]. The development of NPC results from a complex interplay of genetic predisposition [2], environmental influences, and lifestyle factors that collectively contribute to its pathogenesis [3]. Among these, Epstein-Barr virus (EBV) infection plays a central role in both the initiation and progression of the disease [4, 5]. EBV not only infects nasopharyngeal epithelial cells but also interacts with diverse genetic and epigenetic alterations, fostering a tumor microenvironment that is uniquely conducive to malignant transformation. This multifaceted virus-host interplay impacts critical cellular pathways, compromises immune surveillance, and drives oncogenic signaling, ultimately shaping the distinct biological behavior and clinical outcomes observed in NPC [6].

EBV exists in two primary states: latency and lytic reactivation [7]. While latent infection permits viral persistence with minimal viral gene expression, the lytic cycle is marked by robust viral gene transcription and replication [8, 9]. Emerging evidence suggests that even a partial or abortive lytic reactivation can significantly impact tumor progression, aiding in NPC pathobiology [10]. A pivotal player in this reactivation is the immediate-early protein BZLF1(ZEBRA, ZTA), which orchestrates the onset of the lytic cycle [11–13]. Current studies imply that BZLF1-driven reactivation can disrupt cellular homeostasis, trigger epithelial-mesenchymal transition (EMT), and promote immune evasion [6]. By subverting multiple signaling networks, BZLF1 enhance NPC invasiveness and metastatic potential.

Despite therapeutic advances, including radiotherapy and chemotherapy, NPC still shows high rates of recurrence and metastasis, often linked to EBV reactivation events [14-16]. Understanding how EBV reactivation mediates these outcomes is crucial for designing more effective treatment strategies. Here, we aim to systematically elucidate the molecular pathways activated by BZLF1 in NPC during Lytic reactivation. By applying an integrated multi-omics approach, we aimed to identify a candidate gene signature that underpins EBV-driven tumor progression. Our study identified prognostic gene markers associated with EBV reactivation in nasopharyngeal carcinoma by integrating transcriptomic and proteomic analyses. This finding provides new evidence for elucidating the molecular association between EBV and nasopharyngeal carcinoma, which not only deepens the understanding of EBV oncogenic mechanisms, but also provides important clues for clinical diagnosis and therapeutic target development.

#### Materials and methods

## Publicly available datasets and preprocessing

RNA-seq data from NPC patients were obtained from the Gene Expression Omnibus (GEO) database [GSE102349]. After mapping probes to gene symbols based on platform annotations and filtering out probes that mapped to multiple genes, the average expression value was used for genes with multiple probes. Samples missing survival information or with lost follow-up were excluded, leaving 88 NPC patient samples for survival analysis. BZLF1 expression levels were used to stratify patients into risk groups via the `surv\_cutpoint` function in R (version [4.4.1]).

#### Cell lines and culture conditions

NPC43, HK1, and HK1-EBV NPC cell lines were obtained from Prof. George Sai Wah TSAO 's Lab, the University of Hong Kong. NPC43 cells and its sublines were cultured in RPMI 1640 medium supplemented with 10% fetal bovine serum (FBS) (Gibco, Cat. No. [A5256701]), 10  $\mu$ M Y-27,632 (Selleck Chemicals, Cat. No. S1049), and 1% penicillin/streptomycin (ECOTOP, Cat. No. [ES8542]). HK1 and HK1-EBV cells were cultured in RPMI 1640 medium supplemented with 10% FBS and 1% penicillin/streptomycin. All cells were maintained at 37 °C in a humidified atmosphere containing 5%  $\rm CO_2$ .

## Plasmid transfection

Plasmids pcDNA3.1 (Umine-Bio, Cat. No. [YMSW20241210002]) and pcDNA3.1-BZLF1(+) (Umine-Bio, Cat. No. [YMSW20241210001]) were used for transfection. NPC43 cells (2×10<sup>5</sup> per well) were seeded into six-well plates and incubated at 37 °C until reaching 80% confluence. Cells were transfected with 2.5 μg/well of either pcDNA3.1 or pcDNA3.1-BZLF1(+) using Lipo8000™ Transfection Reagent (Beyotime, Cat. No. [C0533]) following the manufacturer's protocol. Forty-eight hours post-transfection, BZLF1 expression was measured via RT-qPCR and Western blot.

# **Real-time PCR**

Total RNA was extracted from NPC cells using TRIzol reagent (Beyotime, Cat. No. [R0016]). cDNA was synthesized using a reverse transcription kit (TOYOBO, Cat. No. [FSQ-301]). RT-qPCR was performed with ChamQ SYBR qPCR Master Mix (Vazyme, Cat. No. [Q331-02]) on a 7500 Real-Time PCR System (Thermo Fisher Scientific, Cat. No. [4351104]). Gene expression levels were normalized to ACTB, and relative expression was calculated using the  $2^{-\Delta}\Delta$ Ct) method.

## Western blot

Proteins were extracted using RIPA lysis buffer (Beyotime, Cat. No. [P0013B]) and quantified by BCA assay (Beyotime, Cat. No. [P0012S]). Protein samples (40  $\mu$ g) were separated by SDS-PAGE and transferred to nitrocellulose membranes (Merck millipore, Cat. No. [IPVH00010]). Membranes were blocked with 5% skim milk in TBST for 30 min and incubated overnight at 4 °C with primary antibodies: anti- $\beta$ -actin (Zenbio, Cat. No. [380624], 1:5000) and anti-EBV ZEBRA (BZLF1) (Santa Cruz Biotechnology, Cat. No. [sc-53904], 1:500). Membranes were then incubated with HRP-conjugated secondary antibodies (Enogene, Cat. No. [E0L3032-1], 1:1000) for 1 h at room temperature. Protein bands were detected using chemiluminescence reagents (Beyotime, Cat. No. [P0018M]) and analyzed via ImageJ software.

# Migration assay

HK1 and HK1-EBV cells were serum-starved for 12 h before being resuspended in RPMI 1640 containing 2% FBS at  $5\times10^5$  cells/mL. A total of 500  $\mu L$  of RPMI 1640 with 10% FBS was added to the lower chamber of a Transwell insert (Beyotime, Cat. No. [FTW061-48Ins], 8  $\mu m$  pore), while 200  $\mu L$  of the cell suspension was added to the upper chamber. Cells were incubated at 37 °C for 24–48 h. After incubation, migrated cells were fixed with 4% paraformaldehyde for 20 min, stained with 0.1% crystal violet, and counted in five randomly selected 10× fields of view under a light microscope.

## CCK8 cell viability assay

NPC43, C17, and HK1-EBV cells were transfected with BZLF1 plasmid. Twenty-four hours post-transfection, cells were trypsinized, resuspended, and seeded at 5000 cells/well in 96-well plates. At 24, 48, and 72 h, 10  $\mu$ L of CCK8 solution (MCE, Cat. No. [HY-K0301]) was added per well and incubated for 2 h at 37 °C. Absorbance was measured at 450 nm using a microplate reader (TECAN, Model [SUNRISE]).

# Flow cytometry

NPC43 and its KO cells were treated with TPA (12-O-tetradecanoylphorbol-13-acetate) or DMSO for 72 h, fixed with 70% ethanol, and stained with PI (Yeasen, Cat. No. [40710ES03]) for cell cycle analysis using flow cytometry (Beckman Coulter, Model [MoFlo XDP]). Data were analyzed using FlowJo (version [10.8.1], https://flowjo.com/flowjo/download). to compare the distribution differences in G0/G1, S, and G2/M phases between the TPA-treated and DMSO control groups. The experiment ensured a final DMSO concentration of  $\leq$  0.1% to avoid solvent toxicity interference.

# RNA-seq and LC-MS/MS

#### RNA-sea

After 48 h of plasmid transfection treatment, total RNA was extracted from NPC43 cells, and mRNA was enriched using oligo(dT) magnetic beads for subsequent cDNA library construction. The library was subjected to paired-end sequencing ( $\geq$ 20 million reads) on the Illumina sequencing platform. Raw data underwent quality control, alignment, and differential expression analysis to identify differentially expressed genes.

## LC-MS/MS

NPC43 cells were treated with 40 ng/mL TPA for 72 h, after which total proteins were extracted and enzymatically digested into peptides. The peptides were then separated using C18 reversed-phase liquid chromatography. High-resolution mass spectrometry was employed to analyze the peptides in liquid chromatography-tandem mass spectrometry (LC-MS/MS) mode, utilizing dataindependent acquisition (DIA). Peptide identification and quantification were performed based on a pre-constructed spectral library or through a direct DIA strategy. Differential gene screening was performed using a two-step method: (1) differential molecules were separately screened from RNA-seq and DIA; (2) genes showing consistent changes in both datasets were selected for subsequent analysis.

# Bioinformatics and statistical analysis

RNA-seq data were aligned to the human genome (hg38) using STAR (version [2.7.10a], [https://github.com/alex dobin/STAR/releases]), and differential expression anal ysis was performed using DESeq2 (version [1.40.2], [htt ps://bioconductor.org/packages/release/bioc/html/DES eq2.html]). Differentiated screening criteria:|log2FC|>1 for transcriptomic data (RNA-seq) to accommodate the broad nature of transcriptional regulation; and a more stringent|log2FC|>1.5 criterion for proteomic data (LC-MS/MS) to reduce mass spectrometry's inherent variability effects. Functional enrichment (Gene Ontology (GO) and KEGG pathway analysis) was conducted using (https://davidbioinformatics.nih.gov/), gene set enrichment analysis (GSEA) was performed using the GSEA software (Broad Institute, version [v4.3.3 for Windows], https://www.gsea-msigdb.org/gsea/dow nloads.jsp). Protein-protein interaction (PPI) networks were constructed with STRING (URL) and visualized using Cytoscape (version [v.3.10.2], https://cytoscape.org /download.html).

Survival analysis was performed using the "survival" package in R. The `surv\_cutpoint` function was used to determine optimal gene expression cutoff points. Kaplan-Meier survival curves were plotted, and differences between groups were assessed using the log-rank test.

Statistical significance between experimental and control groups was determined using a two-tailed Student's t-test with GraphPad Prism 9.5. A p-value of <0.05 was considered statistically significant (\*P<0.05, \*\*P<0.01, \*\*\*P<0.001). Data are presented as mean  $\pm$  SEM.

#### Results

# BZLF1 expression correlates with adverse clinical outcomes

EBV lytic reactivation has been frequently associated with treatment failure and metastasis in nasopharyngeal carcinoma (NPC), as demonstrated in multi-center studies [17, 18]. Previous investigations support the central role of BZLF1-a master regulator of the EBV lytic cycle—in driving NPC aggressiveness. For example, Dochi et al. showed that elevated BZLF1 levels in NPC biopsy samples correlate with higher recurrence rates [19]. In a recent clinical study conducted by Changhua Christian Hospital in Taiwan, the authors stratified stage III NPC patients based on a plasma EBV DNA cutoff of 1000 copies/mL [20] (determined by ROC curve analysis with AUC = 0.6706, P < 0.001, where 826 copies/mL was identified as the optimal cutoff then rounded to 1000 copies/mL for clinical practicality) and demonstrated that patients with high viral loads (≥ 1000 copies/mL) had significantly higher rates of tumor recurrence and distant metastasis (P < 0.01) (Table 1). These findings highlight the clinical relevance of BZLF1 in nasopharyngeal carcinoma (NPC) patients and support the hypothesis that BZLF1 modulates host gene networks to enhance tumor aggressiveness.

To further investigate this hypothesis, we analyzed the GSE102349 dataset, which comprises 113 EBV-positive primary NPC samples (Fig. 1A). After excluding 26 samples due to incomplete survival data or EBNA1 negativity (Fig. 1B), the latter indicating latent EBV infection status incompatible with our lytic reactivation study. we stratified the samples into BZLF1-negative and BZLF1-positive groups using the median expression level of BZLF1 as the cutoff. Kaplan-Meier survival curves and Log-rank

tests revealed a non-significant difference (p = 0.16) toward worse progression-free survival (PFS) in the BZLF1-positive group (n = 45) compared to the BZLF1-negative group (n = 42) (Fig. 1C). Subgroup analyses in 87 patients further indicated that, in undifferentiated tumors (n = 19 of 36, p < 0.24) and type I tumors (n = 25 of 50, p < 0.3), BZLF1-positive cohorts tended to have poorer prognoses. Although these trends did not reach statistical significance—likely due to sample size limitations—they suggest that elevated pEBV DNA levels, reflecting EBV reactivation, may contribute to increased tumor recurrence, enhanced metastatic potential, and more aggressive NPC progression.

# Elevated BZLF1 expression drives aggressive metastatic behaviour in NPC cells

To elucidate its role in tumor progression, we established a robust in vitro EBV reactivation model using NPC43 cells. In this system, cells were transfected with a BZLF1expressing plasmid or treated with TPA (12-O-tetradecanoylphorbol-13-acetate) to establish an EBV lytic reactivation model. Next, we performed RT-qPCR and Western blot analyses and observed robust upregulation of BZLF1 at both the mRNA and protein levels (Fig. 2A), consistent with recent literature underscoring its pivotal role in EBV reactivation and tumor progression [19]. Next, we performed comprehensive RNA sequencing and LC-MS/MS profiling of the reactivated cells. RNAseq analysis identified 106 differentially expressed genes (82 upregulated and 24 downregulated; Figs. 2B-C), reflecting profound transcriptional reprogramming. GO enrichment analysis revealed that these changes predominantly affected pathways involved in endoplasmic reticulum stress, viral gene regulation, glycolysis, and protein folding (Fig. 2D), while KEGG pathway analysis highlighted enrichment in protein processing, metabolic reprogramming, leukocyte transendothelial migration, ferroptosis, hypoxia, and virus-induced carcinogenesis (Fig. 2E). Moreover, Gene set enrichment

Table 1 Summary of failure site(s) in 106 patients with high EBV DNA level vs. 250 patients with low EBV DNA level

Failure site(s)	Pretreatment EBV DNA level subgroup				
		Total n = 365	Low EBV DNA level subgroup (<1000 copies/ml) n=250	High EBV DNA level subgroup (≥ 1000 copies/ml)  n=106	Pvalues
	_				
Primary Tumor	Т	22	15	7	/
Metastatic lymph nodes	N	5	2	3	1
Distant metastases	M	26	11	15	/
Regional cancer	T + N	3	1	2	/
Distantly situated cancer	T + M	6	1	5	1
	N + M	3	1	2	/
	T + N + M	1	0	1	/
The sum total of any failures		66	31	35	<0.01
Total number of M-level failures		36	13	23	<0.01

Luo et al. Journal of Translational Medicine (2025) 23:616 Page 5 of 12

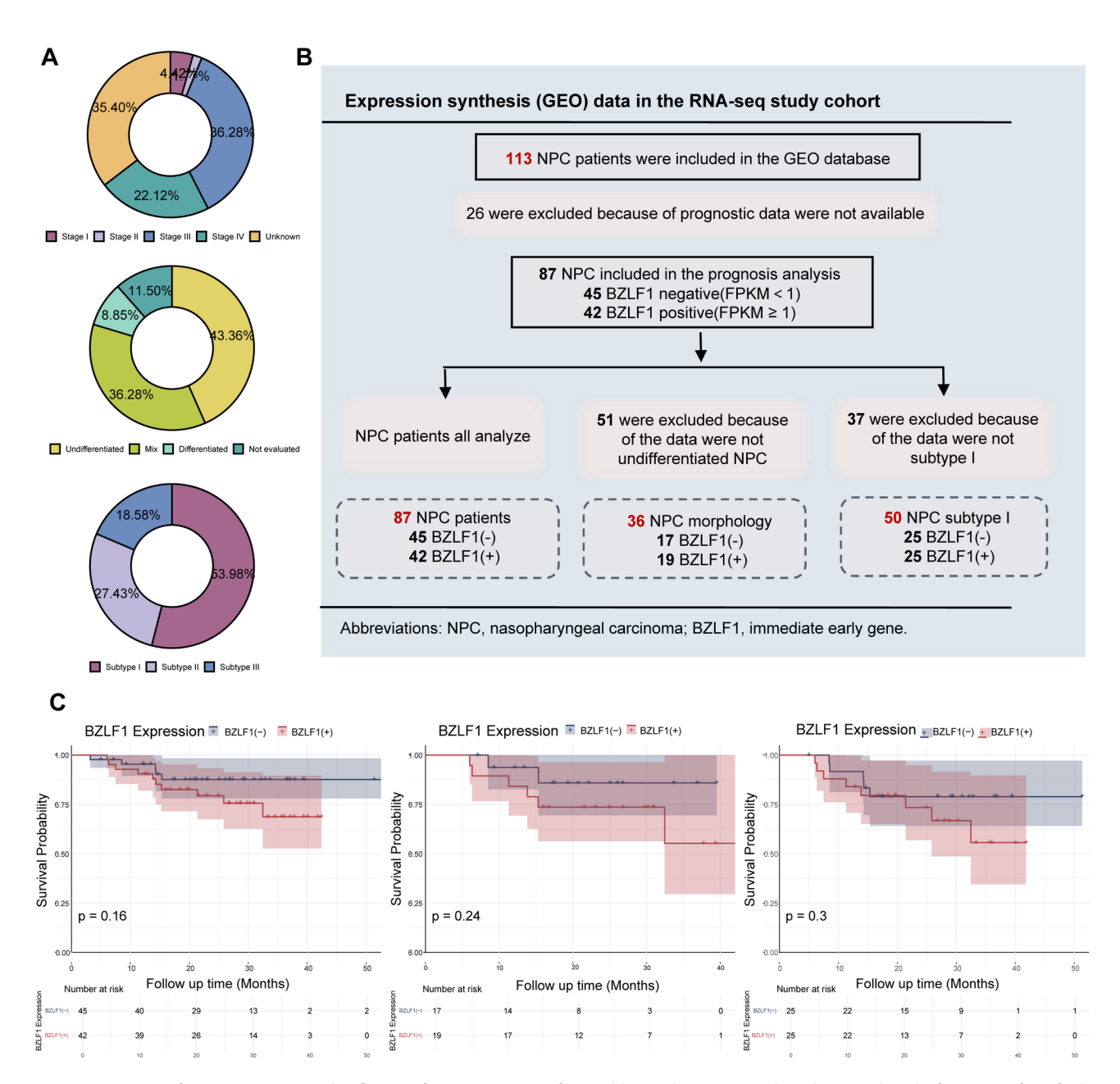


**Fig. 1** Acquisition of NPC Patient Data and Definition of Screening Criteria from Public Databases. (**A**) Pie chart showing clinical information of 113 fresh nasopharyngeal carcinoma patient samples divided into three groups: clinical stage, tumor differentiation type, and subtype.(**B**) A selection diagram based on high- and low-expression scoring criteria for BZLF1. (**C**) Survival analysis, differential expression profiles across tumor cell differentiation and subtype-specific expression patterns between BZLF1-negative and BZLF1-positive groups. Statistical significance is defined as *p* < 0.05

analysis revealed significant activation of pathways involving EMT, NF-κB signaling, hypoxia response, and inflammation (Fig. 2F). These pathways collectively establish a metastatic network through HIF-mediated matrix remodeling, inflammation-driven MMPs release, and EMT-CTGF synergy [21].

Using Cytoscape for network visualization (Fig. 2G), we identified increased activity in pathways such as mTOR signaling, ribosome biogenesis, and glycolysis/gluconeogenesis, along with a clear downregulation of

pathways related to oxidative phosphorylation, cell cycle regulation, and gap junction formation. To validate these molecular insights, we assessed cell proliferation using CCK8 assays (Fig. 2H) but observed no significant differences (P = 0.13) between BZLF1-overexpressing cells and controls. This finding led us to hypothesize that BZLF1 might influence cell cycle regulation.

To test this hypothesis, we performed flow cytometry analysis, which revealed a significant 15.6% increase in the proportion of cells in the S+G2/M phases in

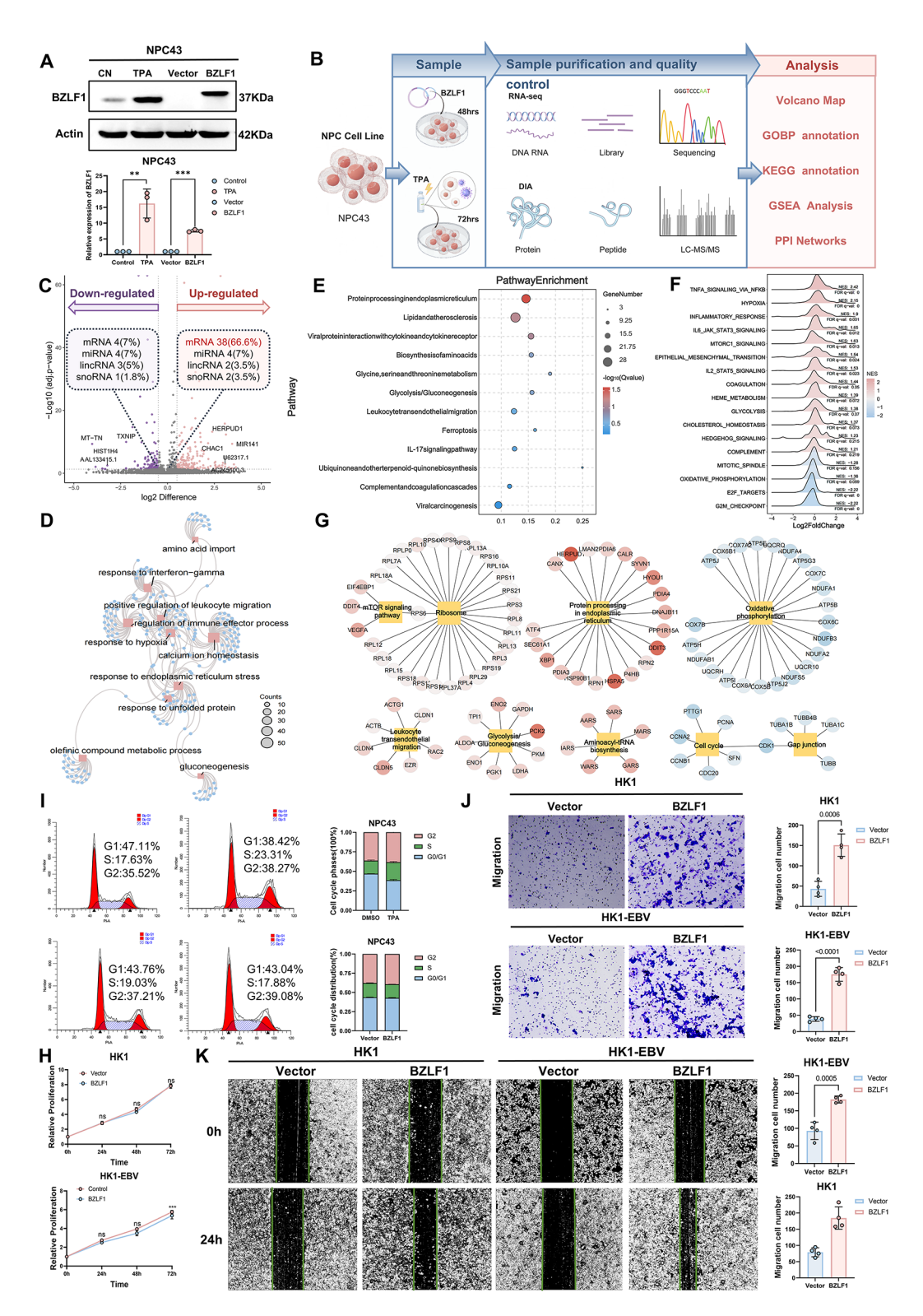


Fig. 2 (See legend on next page.)

TPA-treated cells compared to DMSO-treated controls (Fig. 2I). However, in BZLF1-overexpressing cells, the proportion of cells in the S+G2/M phases was 56.96%, which was not significantly different from the 56.24%

observed in vector-transfected cells. Combined with CXCR4 regulatory studies, which promote G2/M blockade through negative regulation of BZLF1, although the EBV-encoded BZLF1 protein partially enhances tumor

Luo et al. Journal of Translational Medicine (2025) 23:616 Page 7 of 12

(See figure on previous page.)

Fig. 2 EBV lysis reactivation model promotes metastasis and induces cell cycle arrest in NPC cells. (A) Validation of BZLF1 overexpression on gene and protein levels in NPC43 cells using RT-qPCR and Western blotting. \* p < 0.05, Control vs. TPA, Vector vs. BZLF1, Student's t-test; (B) Determine the experimental design and workflow of the NPC43-induced EBV lysis reactivation proteome and transcriptome in NPC cells; (C) Volcano plots of RNA-seq differential genes show the types and percentages of genes that are up-regulated (red) and down-regulated (purple); the top 5 genes in each category are labeled; (D) Examples of GOBP functional annotations for differential genes (one-sided Fisher's exact test, p < 0.05). Boxes highlight the relevant enriched term (red), and the size of the box represents the significance of enrichment. Blue dots represent the involved genes. (E) Representative KEGG function annotations for differential genes (one-sided Fisher's exact test, p < 0.05). The size of the dots reflects the number of proteins associated with the relevant term. Color bars represent the significance of enrichment; (F) Gene set enrichment analysis (GSEA) mountain range plot of all mRNAs in transcriptomics based on Hallmark gene sets. Red color indicates positively enriched pathways and blue color indicates negatively enriched pathways. Pathway names are organized by FDR value; (G) Metabolic pathway network diagram produced using Cytoscape showing 8 metabolic pathways, metabolic pathway names (yellow), genes with increased expression (red) and genes with decreased expression (blue), with the color shade correlating with the change in log2FC values of the genes, with the larger the absolute value, the darker the color; (H) Cell viability of BZLF1 overexpressing HK1 versus HK1-EBV cells as determined by CCK8. \*\*\*p < 0.005, Vector and BZLF1, Student's t-test; (I) Cell cycle analysis of BZLF1 overexpressing NPC43 cells analyzed by flow cytometry using PI staining. DMSO with TPA, Vector and BZLF1; (J) Representative Transwell invasion assay images showing vector versus BZLF1-expressing HK1 and HK1-EBV cells (left panel), comparative quantitative analysis of invasive cell counts (right panel); (K) Light microscopic examination of wound healing assay in HK1 and HK1-EBV cells with different BZLF1 expression levels. Magnification 40×, bar = 200 µm. Vector with BZLF1 at 24 h, Student's t-test

cell proliferation, it has a weak regulatory effect on the G2/S phase checkpoint, suggesting that this viral protein is not a key factor for cell cycle regulation in nasopharyngeal carcinoma progression.

In contrast, both wound healing and Transwell migration assays (Figs. 2J-K) demonstrated that elevated BZLF1 expression significantly enhanced the migratory capacity of nasopharyngeal carcinoma (NPC) cells. These findings provide strong evidence that BZLF1 directly promotes tumor metastasis. The experimental data clearly demonstrate that BZLF1 overexpression significantly enhances the migratory capacity of NPC cells (p<0.01), directly confirming its critical regulatory role in promoting tumor metastatic potential through facilitating cell migration. Furthermore, they align with clinical observations linking BZLF1 expression to tumor aggressiveness, suggesting that epithelial-mesenchymal transition (EMT) and cell cycle modulation are critical downstream events in EBV-mediated tumor progression.

In summary, by integrating transcriptomic and proteomic analyses, we found that BZLF1 expression not only reprograms key cellular pathways but also imparts a more aggressive, migratory phenotype in NPC cells. These findings highlight the potential of targeting BZLF1 to mitigate EBV-associated tumor progression and provide a mechanistic basis for its role in driving tumor aggressiveness and metastasis.

# Identification and functional analysis of a ten-gene signature

To refine our candidate gene list and gain deeper insights into EBV-mediated oncogenesis in nasopharyngeal carcinoma (NPC), we integrated RNA-seq and LC-MS/MS data from reactivated NPC43 cells. RNA-seq analysis identified 161 differentially expressed genes (DEGs) ( $|\log_2\text{FoldChange}| > 1$ , adjusted p < 0.05), while LC-MS/MS profiling revealed 428 differentially expressed proteins (DEPs) ( $|\log_2\text{FoldChange}| > 1.5$ , adjusted p < 0.05). By converging transcriptional and proteomic datasets, we

minimized false positives and highlighted putative "drivers" of EBV-induced malignancy. Venn diagram analysis revealed nine consistently upregulated genes—PLAUR, SBSN, LAMC2, CDC42EP1, S100P, F3, CYP24A1, KRT6B, and PTGS2—and one consistently downregulated gene, NQO1 (Figs. 3A–B). While several of these genes (e.g., LAMC2, PTGS2) have established roles in solid tumors, their coordinated upregulation under EBV reactivation conditions adds a new dimension to NPC pathobiology.

GO functional analysis indicated that these candidate genes are predominantly associated with apoptosis signaling, oxidative stress, hypoxia, pyridine nucleotide metabolism, and NAD metabolism (Fig. 3C), while KEGG pathway analysis highlighted enrichment in protein processing, metabolic reprogramming, leukocyte transendothelial migration, ferroptosis, hypoxia, and virus-induced carcinogenesis. Network and functional enrichment analyses linked these genes to diverse oncogenic pathways, including complement and coagulation cascades (F3), keratin complex remodeling (KRT6B), laminin matrix interactions (LAMC2), and metabolic reprogramming (CYP24A1, NQO1). Protein-protein interaction networks constructed using the STRING database and visualized with Cytoscape (Fig. 3D) grouped these genes into distinct functional clusters; notably, F3 exhibited the highest interaction activity by regulating complement and coagulation cascades, with PLAUR contributing significantly. Additionally, a cluster linked to ubiquinone and terpenoid quinone biosynthesis predominantly comprised NQO1 and PTGS2, while structural genes KRT6B and LAMC2 emerged as key players in epidermal structure formation and laminin complex assembly.

Next, to assess the clinical relevance of these candidates, we analyzed expression scores using clinical data from 88 NPC patients. Patients were stratified into high-and low-expression groups, and heatmap analysis of the five most consistent samples revealed elevated expression of EMT-related genes coupled with downregulation of

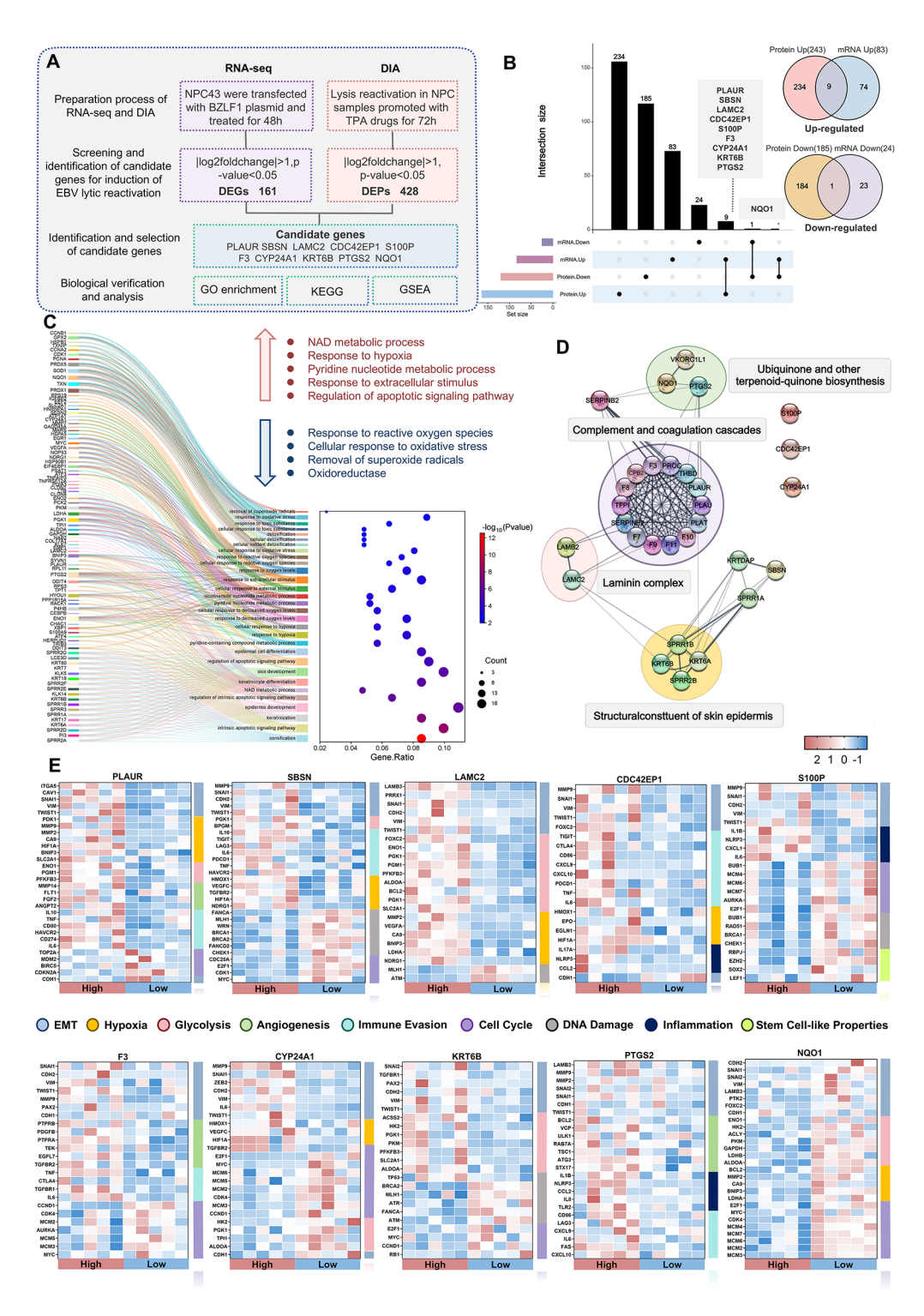


**Fig. 3** Candidate gene cluster screening and its functional analysis. (**A**) Conditional threshold and workflow for joint transcriptomics and proteomics screening of candidate genes or proteins; (**B**) UP-set plots combined with Venn diagrams show the distribution of genes and proteins in different subgroups. Candidate gene screening criteria are based on synchronized up-regulated (red) and synchronized down-regulated subgroups (blue); (**C**) Representative GOBP functionally annotated Mulberry plots of candidate gene families (one-sided Fisher's exact test, *p* < 0.05). The dot size represents the number of proteins associated with the relevant term, while the colour bars denote the level of enrichment significance. Top five up-regulated pathways (red) and top four down-regulated pathways (blue); (**D**) Protein interaction information of candidate gene families was collected using the STRING database and protein interaction networks (PPIs) were mapped by Cytoscape. k-means clustering analysis delineated four major functional clusters; (**E**) Heatmap analysis of candidate genes in groups of high and low expression, each group contains five samples from NPC patients, and the distribution of the corresponding pathways is indicated by different colors in the right matrix plot

Luo et al. Journal of Translational Medicine (2025) 23:616 Page 9 of 12

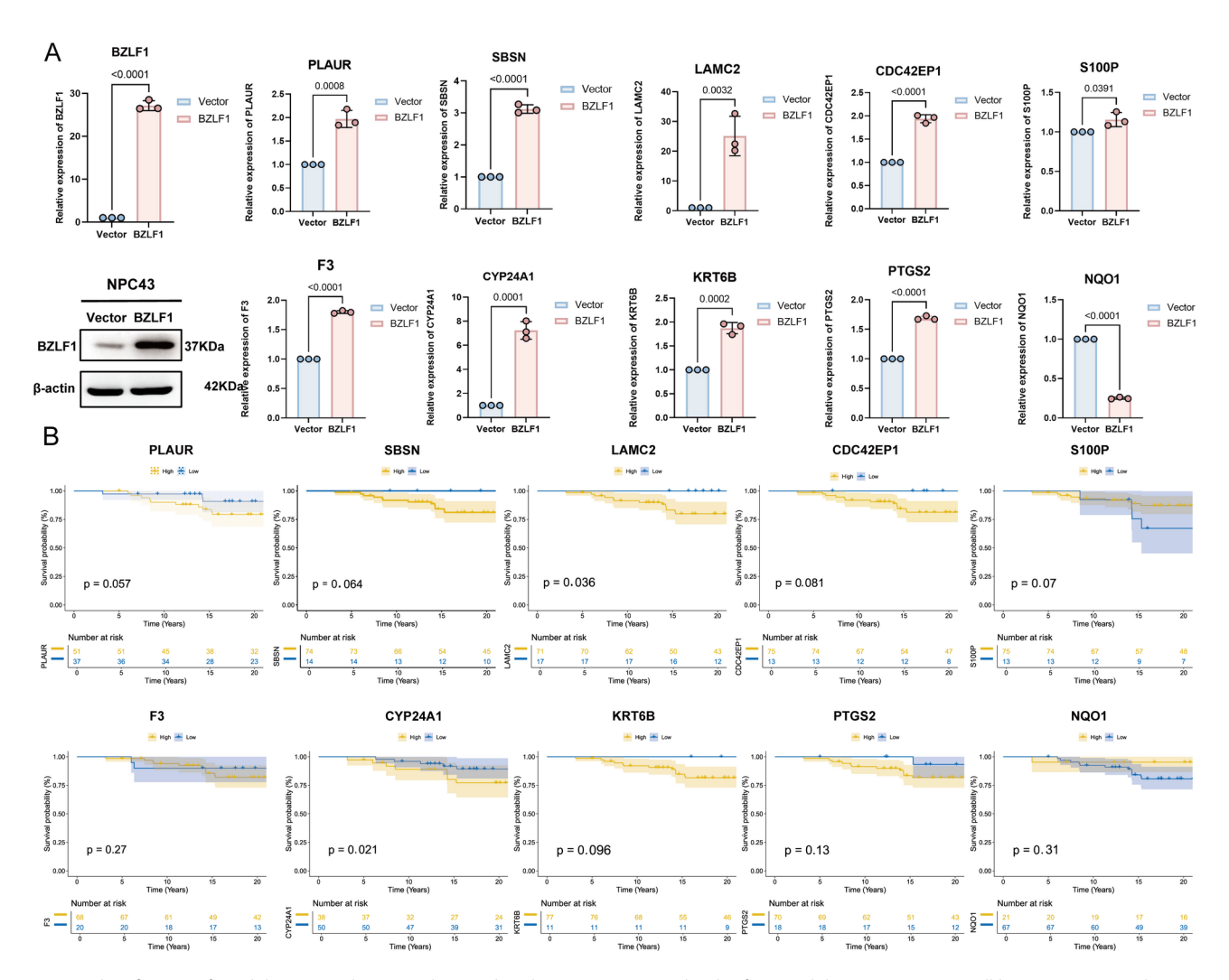


**Fig. 4** Identification of candidate gene clusters and survival analysis. (**A**) Expression levels of 10 candidate genes in NPC cell lines were assessed using RT-qPCR, with the experiments divided into Vector and BZLF1 plasmid transfection groups, Student's t-test; (**B**) Survival curve analysis: the 10 candidate genes were classified into high and low expression groups according to the survival score, and their prognostic relationships were evaluated

cell cycle-related genes (Fig. 3E). Furthermore, glycolysis-related genes such as PLAUR, SBSN, LAMC2, and CDC42EP1 were significantly regulated, whereas NQO1 exhibited an notably significant reduction during EBV reactivation—suggesting that its downregulation may contribute to NPC progression via non-traditional pathways, potentially by enhancing glycolytic function.

Collectively, by intersecting the DEGs with the DEPs, we refined our candidate list to a ten-gene panel—PLAUR, SBSN, LAMC2, CDC42EP1, F3, S100P, CYP24A1, KRT6B, PTGS2, and NQO1. Network and enrichment analyses revealed that these genes converge on processes critical for NPC metastasis, including extracellular matrix remodeling, oxidative stress responses, and immune evasion. Notably, the negative regulation of NQO1 during EBV lytic reactivation may exacerbate oxidative stress, thereby synergizing with other oncogenic signals to enhance tumor aggressiveness. In summary,

our integrative multi-omics approach not only refines large-scale datasets into a focused subset of potential "driver" genes but also highlights the novelty of a coordinated gene signature under EBV reactivation—providing fresh insights into the viral-driven pathophysiology of NPC.

# Clinical validation and prognostic significance of the tengene signature

To validate the expression patterns identified through RNA sequencing, we performed RT-qPCR analysis using RNA extracted from our in vitro EBV reactivation model. The RT-qPCR results demonstrated concordance with the RNA-seq data, confirming the differential expression of all ten signature genes during EBV reactivation (Fig. 4A). Further validation was conducted using the GSE102349 dataset comprising 88 NPC patient samples. Survival analysis revealed that elevated expression of

CYP24A1 (p = 0.021) and LAMC2 (p = 0.036) were significantly associated with poor prognosis. While the remaining signature genes (KRT6B, SBSN, PTGS2, PLAUR, and CDC42EP1) showed similar trends toward reduced survival, these associations did not reach statistical significance, which may be influenced by several factors such as sample size and patient heterogeneity. Notably, decreased expression levels of S100P and F3 demonstrated a potential association with malignant progression, showing a trend toward statistical significance (p = 0.08 and p = 0.27, respectively). While decreased NQO1 expression correlated with unfavorable prognosis, though not reaching statistical significance (p = 0.31).

The validated gene signature encompasses multiple critical pathways in NPC pathogenesis, including metabolism, migration, immune escape, EMT, oxidative stress response, and hypoxia adaptation. These findings suggest potential therapeutic strategies targeting specific molecular pathways, such as the hyperactivated coagulation system (through F3/PLAUR) or disrupted oxidative stress responses (via NQO1). Moreover, our results indicate that combining EBV-targeted interventions with approaches targeting these metabolic and migratory processes could potentially enhance NPC treatment efficacy. The clinical validation of this ten-gene signature not only reinforces its prognostic value but also highlights its potential utility in identifying novel therapeutic targets for improved NPC management.

#### Discussion

Our findings provide significant insight into the role of EBV reactivation in NPC, particularly through the function of the immediate-early protein BZLF1. Traditionally, the viral lytic cycle was considered an antagonistic event in tumorigenesis, as full viral replication typically results in host cell lysis [22, 23]. However, increasing evidence suggests that abortive lytic reactivation contributes to tumor progression, allowing viral gene expression while evading complete immune recognition [23, 24]. In this study, we demonstrated that BZLF1 reprograms host cellular pathways, affecting key biological mechanisms such as epithelial-mesenchymal transition (EMT), metabolic adaptation, and immune evasion.

Genomic instability is a hallmark of tumorigenesis [25], and our results indicate that BZLF1 may contribute to this process in NPC [10, 11]. Previous studies have shown that BZLF1 can alter chromatin structure and modulate host transcriptional networks, potentially leading to chromosome mis-segregation and DNA damage [26]. Our transcriptomic and proteomic analyses support this notion, revealing dysregulated pathways related to DNA repair and genomic integrity. The presence of such genomic alterations may promote tumor heterogeneity and contribute to therapeutic resistance, emphasizing the

need for targeted interventions aimed at stabilizing the genome in EBV-positive NPC.

Another major finding of this study is the impact of BZLF1 on EMT, a critical process in cancer metastasis [10, 11]. EMT involves the loss of epithelial characteristics and the acquisition of mesenchymal properties, allowing cells to detach, invade, and migrate [27]. Our study identified that BZLF1 upregulates MMP9 and MMP3, key matrix metalloproteinases involved in extracellular matrix degradation [28]. These findings align with previous reports demonstrating that EBV infection enhances EMT through both viral and host gene interactions. The upregulation of laminin y2 (LAMC2) and suprabasin (SBSN) further supports this hypothesis, as these proteins play integral roles in cell adhesion and migration [29-31]. Collectively, these data suggest that EBV reactivation facilitates NPC metastasis, highlighting potential therapeutic targets to inhibit EMT-driven tumor progression.

Metabolic reprogramming is another key hallmark of cancer, allowing tumor cells to adapt to hostile microenvironments [32–34]. We observed that EBV reactivation enhances glycolysis, a well-known metabolic adaptation in NPC [35]. The increased expression of CYP24A1 (Cytochrome P450 Family 24 Subfamily A Member 1), which plays a role in vitamin D metabolism, may further contribute to metabolic shifts, particularly in protecting tumor cells from ferroptosis, a form of iron-dependent cell death [36]. By evading ferroptosis, NPC cells may enhance their survival under oxidative stress, thus promoting tumor aggressiveness [37]. The metabolic changes induced by EBV reactivation also suggest potential vulnerabilities that could be exploited for therapeutic intervention, particularly in disrupting glycolytic pathways or inducing ferroptosis as a targeted treatment strategy.

Our findings further illustrate that EBV reactivation plays a role in modulating coagulation and immune evasion mechanisms in NPC [26, 38]. The upregulation of tissue factor (F3) and urokinase-type plasminogen activator receptor (PLAUR) indicates that EBV-positive NPC tumors may create a pro-thrombotic microenvironment [39, 40], which can facilitate tumor growth, angiogenesis, and metastasis [41]. This supports previous research showing that hypercoagulability in cancer patients is associated with worse prognosis and increased metastatic potential [40]. Additionally, the modulation of immune pathways suggests that EBV reactivation may enable NPC cells to evade immune surveillance [26]. The downregulation of NAD(P)H: quinone oxidoreductase 1 (NQO1), a key player in oxidative stress response [42], raises the possibility that EBV-positive tumors exploit redox imbalances to further suppress immune detection and enhance survival [43].

S100 calcium-binding protein P (S100P), an established oncogene in several malignancies [44], exhibited unique behavior in NPC. While its high expression is often correlated with tumor progression [45–47], our analysis suggests a context-dependent role in NPC, possibly influenced by the EBV-positive tumor microenvironment. The functional plasticity of S100P indicates that its role in NPC may differ from other cancers, warranting further investigation into its precise regulatory mechanisms in EBV-driven oncogenesis.

While our findings provide critical insights, certain limitations must be acknowledged. The sample size, though sufficient for initial analyses, warrants expansion to validate our findings in larger, more diverse cohorts. Additionally, while transcriptomic and proteomic analyses offer powerful tools to uncover gene expression changes, functional studies such as in vivo models, ChIP-seq, and immunohistochemical validation are necessary to confirm the mechanistic contributions of BZLF1 and its downstream targets. Future studies should also explore therapeutic interventions that disrupt the pathways identified in our study, with a focus on metabolic vulnerabilities, EMT inhibition, and immune-targeted approaches.

In conclusion, our study highlights the oncogenic role of BZLF1 in NPC during EBV reactivation. By leveraging transcriptomic and proteomic analyses, we have elucidated how BZLF1 contributes to EMT, metabolic reprogramming, immune evasion, and genomic instability. These findings provide a foundation for developing targeted therapies that mitigate EBV-driven oncogenesis, with potential applications in precision medicine for NPC patients. Future research should focus on further validating these pathways and identifying effective strategies to counteract the oncogenic effects of EBV reactivation in NPC.

#### **Author contributions**

Qingshuang Luo and Jingyi Long: Conceptualization, Methodology, Software, Data curation, Writing-Original draft preparation. Longtai Hu: Methodology, Visualization, Investigation. Moyed Alsaadawe: Software. Oluwasijibomi Damola Faleti: Writing- Reviewing and Editing. Xiaoming Lyu: Supervision, Validation, Writing- Reviewing and Editing, Project administration and Funding acquisition.

# Funding

The work was partially supported by grants from Guangdong Basic and Applied Basic Research Foundation, China (2021A1515010713); President Foundation of the Third Affiliated Hospital, Southern Medical University (YM2021001);

## Data availability

The datasets used and/or analyzed during the current study are available from the GEO database or from corresponding author on reasonable request.

## **Declarations**

#### Conflict of interest

The authors declare no conflict of interest.

Received: 27 March 2025 / Accepted: 29 April 2025 Published online: 02 June 2025

#### References

- Tsao SW, Tsang CM, Lo KW. Epstein-Barr virus infection and nasopharyngeal carcinoma. Philos Trans R Soc Lond B Biol Sci. 2017;372(1732):20160270. https://doi.org/10.1098/rstb.2016.0270
- Z. Y et al., "Whole-exome sequencing association study reveals genetic effects on tumor microenvironment components in nasopharyngeal carcinoma.' J Clin Invest, 2025;135, 1, https://doi.org/10.1172/JC1182768
- Su ZY, Siak PY, Lwin YY, Cheah S-C. 'Epidemiology of nasopharyngeal carcinoma: current insights and future outlook,' Cancer Metastasis Rev., 2024;43(3):919–939, https://doi.org/10.1007/s10555-024-10176-9
- Lee Y-CG, et al. Effect of Epstein-Barr virus infection on global gene expression in nasopharyngeal carcinoma. Funct Integr Genomics. 2007;7(1):79–93. https://doi.org/10.1007/s10142-006-0035-2
- Yang L, Liu G, Li Y, Pan Y. The emergence of tumor-infiltrating lymphocytes in nasopharyngeal carcinoma: Predictive value and immunotherapy implications', Genes Dis., 2022;9(5):1208–1219, https://doi.org/10.1016/j.gendis.2021. 07.002
- SoRelle ED, et al. Epstein-Barr virus reactivation induces divergent abortive, reprogrammed, and host shutoff States by lytic progression. PLOS Pathog. 2024;20(10):e1012341. https://doi.org/10.1371/journal.ppat.1012341
- Murata T, Tsurumi T. Switching of EBV cycles between latent and lytic States. Rev Med Virol. 2014;24(3):142–53. https://doi.org/10.1002/rmv.1780
- Ersing I, et al. A Temporal proteomic map of Epstein-Barr virus lytic replication in B cells. Cell Rep. 2017;19(7):1479–93. https://doi.org/10.1016/j.celrep.2017.0 4.062
- Morales-Sánchez A, Fuentes-Panana EM. The Immunomodulatory Capacity of an Epstein-Barr Virus Abortive Lytic Cycle: Potential Contribution to Viral Tumorigenesis', Cancers, 2018;10(4):E98, https://doi.org/10.3390/cancers1004 0098
- Germini D et al. Jun, "Oncogenic Properties of the EBV ZEBRA Protein," Cancers, 2010;12(6):E1479, https://doi.org/10.3390/cancers12061479
- Speck SH, Chatila T, Flemington E. 'Reactivation of Epstein-Barr virus: regulation and function of the BZLF1 gene', Trends Microbiol., 1997;5(10):399–405, https://doi.org/10.1016/S0966-842X(97)01129-3
- Chevallier-Greco A, Manet E, Chavrier P, Mosnier C, Daillie J, Sergeant A. 'Both Epstein-Barr virus (EBV)-encoded trans-acting factors, EB1 and EB2, are required to activate transcription from an EBV early promoter', EMBO J, 1986;5(12):3243–3249, https://doi.org/10.1002/j.1460-2075.1986.tb04635.x
- Petosa C, Morand P, Baudin F, Moulin M, Artero J-B, Müller CW. 'Structural basis of lytic cycle activation by the Epstein-Barr virus ZEBRA protein', Mol. Cell, 2006;21(4):565–572, https://doi.org/10.1016/j.molcel.2006.01.006
- Wang F-H et al. Mar., 'Efficacy, Safety, and Correlative Biomarkers of Toripalimab in Previously Treated Recurrent or Metastatic Nasopharyngeal Carcinoma: A Phase II Clinical Trial (POLARIS-02)', J. Clin. Oncol. Off. J. Am. Soc. Clin. Oncol., 2021;39,(7):704–712, https://doi.org/10.1200/JCO.20.02712
- Mai H-Q et al. Sep., 'Toripalimab or placebo plus chemotherapy as first-line treatment in advanced nasopharyngeal carcinoma: a multicenter randomized phase 3 trial', Nat. Med., 2021;27(9):1536–1543, 2021, https://doi.org/10.1 038/s41591-021-01444-0
- Mai H-Q et al. Nov., 'Toripalimab Plus Chemotherapy for Recurrent or Metastatic Nasopharyngeal Carcinoma: The JUPITER-02 Randomized Clinical Trial', JAMA, 2023;330(20):1961–1970, https://doi.org/10.1001/jama.2023.20181
- Sausen DG, Bhutta MS, Gallo ES, Dahari H, Borenstein R. Stress-Induced Epstein-Barr Virus Reactivation, Biomolecules, 2021;11(9):9, https://doi.org/10. 3390/biom11091380
- Lim DW-T, et al. Clinical efficacy and biomarker analysis of dual PD-1/CTLA-4 Blockade in recurrent/metastatic EBV-associated nasopharyngeal carcinoma. Nat Commun. 2023;14(1):2781. https://doi.org/10.1038/s41467-023-38407-7
- Dochi H et al. Aug., 'Estrogen induces the expression of EBV lytic protein ZEBRA, a marker of poor prognosis in nasopharyngeal carcinoma', Cancer Sci., 2022;113(8):2862–2877, https://doi.org/10.1111/cas.15440
- Twu C-W, et al. Effects of Epstein-Barr virus viral load and different treatment modality for stage III nasopharyngeal carcinoma. Head Neck. 2020;42(8):1765–74. https://doi.org/10.1002/hed.26096
- Finger EC, Giaccia AJ. Hypoxia, inflammation, and the tumor microenvironment in metastatic disease. Cancer Metastasis Rev. 2010;29(2):285–93. https://doi.org/10.1007/s10555-010-9224-5

- Habib M, et al. Lytic EBV infection investigated by detection of soluble Epstein-Barr virus ZEBRA in the serum of patients with PTLD. Sci Rep. 2017;7(1):10479. https://doi.org/10.1038/s41598-017-09798-7
- M. C, 'Latency and lytic replication in Epstein-Barr virus-associated oncogenesis'. Nat Rev Microbiol, 2019;17(11), https://doi.org/10.1038/s41579-019-024 9-7
- Shi F, et al. Epstein-Barr virus-driven metabolic alterations contribute to the viral lytic reactivation and tumor progression in nasopharyngeal carcinoma. J Med Virol. 2024;96(5):e29634. https://doi.org/10.1002/jmv.29634
- As CXA, J L, D. M, and, Sf B. Chromosomal instability as a driver of cancer progression. Nat Rev Genet. 2025;26(1). https://doi.org/10.1038/s41576-024-0 0761-7
- Buschle A et al. Apr., 'Epstein-Barr virus inactivates the transcriptome and disrupts the chromatin architecture of its host cell in the first phase of lytic reactivation', Nucleic Acids Res., 2021;49(6):3217–3241, https://doi.org/10.109 3/nar/qkab099
- Nieto MA, Huang RY-J, Jackson RA, Thiery JP. EMT: 2016, Cell, 2016;166(1):21–45. https://doi.org/10.1016/j.cell.2016.06.028
- Yoshizaki T, Sato H, Murono S, Pagano JS, Furukawa M. 'Matrix metalloproteinase 9 is induced by the Epstein-Barr virus BZLF1 transactivator', Clin. Exp. Metastasis, 1999;17(5):431–436, https://doi.org/10.1023/a:1006699003525
- Pribyl M et al. Oct., 'Aberrantly elevated suprabasin in the bone marrow as a candidate biomarker of advanced disease state in myelodysplastic syndromes', Mol. Oncol., 2020;14(10):2403–2419, https://doi.org/10.1002/1878-02 61.12768
- Hubackova S et al. Jul., 'Interferon-regulated suprabasin is essential for stress-induced stem-like cell conversion and therapy resistance of human malignancies', Mol. Oncol., 2019;13(7):1467–1489, https://doi.org/10.1002/187 8-0261.12480
- 31. Alam MT, et al. Suprabasin as a novel tumor endothelial cell marker. Cancer Sci. 2014;105(12):1533–40. https://doi.org/10.1111/cas.12549
- Liu Q, Bode AM, Chen X, Luo X. Metabolic reprogramming in nasopharyngeal carcinoma: mechanisms and therapeutic opportunities. Biochim Biophys Acta Rev Cancer. 2023;1878(6):189023. https://doi.org/10.1016/j.bbcan.2023.1 89023
- Yee TM, Wang LW. Metabolic reprogramming in epstein-barr virus associated diseases. J Med Virol. 2025;97:e70197. https://doi.org/10.1002/jmv.70197. no.
- Yang T, You C, Meng S, Lai Z, Ai W, Zhang J. EBV infection and its regulated metabolic reprogramming in nasopharyngeal tumorigenesis. Front Cell Infect Microbiol. 2022;12:935205. https://doi.org/10.3389/fcimb.2022.935205
- Guo R, et al. Methionine metabolism controls the B cell EBV epigenome and viral latency. Cell Metab. Sep. 2022;34(9):1280–e1297. https://doi.org/10.1016 /j.cmet.2022.08.008

- Duan J et al. Jul., "USP11-mediated LSH deubiquitination inhibits ferroptosis in colorectal cancer through epigenetic activation of CYP24A1, Cell Death Dis., 2023;14(7):402, https://doi.org/10.1038/s41419-023-05915-9
- Yuan L, et al. EBV infection-induced GPX4 promotes chemoresistance and tumor progression in nasopharyngeal carcinoma. Cell Death Differ. 2022;29(8):1513–27. https://doi.org/10.1038/s41418-022-00939-8
- Yiu SPT, Zerbe C, Vanderwall D, Huttlin EL, Weekes MP, Gewurz BE. 'An Epstein-Barr virus protein interaction map reveals NLRP3 inflammasome evasion via MAVS UFMylation', Mol. Cell, 2023;83(13):2367–2386.e15, https://doi.org/10.10 16/i.molcel.2023.05.018
- Duan X et al. Mar., 'EBV Infection in Epithelial Malignancies Induces Resistance to Antitumor Natural Killer Cells via F3-Mediated Platelet Aggregation', Cancer Res., 2022;82(6):1070–1083, https://doi.org/10.1158/0008-5472.CAN-21-2292
- Fu Z et al. Feb., 'Identifying PLAUR as a Pivotal Gene of Tumor Microenvironment and Regulating Mesenchymal Phenotype of Glioblastoma', Cancers, 2024;16(4):840, https://doi.org/10.3390/cancers16040840
- 41. Saidak Z, et al. A pan-cancer analysis of the human tumor coagulome and its link to the tumor immune microenvironment. Cancer Immunol Immunother CII. 2021;70(4):923–33. https://doi.org/10.1007/s00262-020-02739-w
- Yu J, et al. Fighting drug-resistant lung cancer by induction of NAD(P)
   H:quinone oxidoreductase 1 (NQO1)-mediated ferroptosis. Drug Resist
   Updat. 2023;70:100977. https://doi.org/10.1016/j.drup.2023.100977
- Liu K, et al. NQO1 stabilizes p53 in response to Oncogene-Induced senescence. Int J Biol Sci. 2015;11:762–71. https://doi.org/10.7150/ijbs.11978
- Gross SR, Sin CGT, Barraclough R, Rudland PS. Joining S100 proteins and migration: for better or for worse, in sickness and in health. Cell Mol Life Sci CMLS. 2014;71(9):1551–79. https://doi.org/10.1007/s00018-013-1400-7
- Geng Y, Li Y, Liu G, Jiao J. Identification of biomarkers for the diagnosis in colorectal polyps and metabolic dysfunction-associated steatohepatitis (MASH) by bioinformatics analysis and machine learning. Sci Rep. 2024;14(1):29463. https://doi.org/10.1038/s41598-024-81120-8
- Sun Y, et al. RBMS1 coordinates with the m6A reader YTHDF1 to promote NSCLC metastasis through stimulating S100P translation. Adv Sci Weinh Baden-Wurtt Ger. 2024;11(15):e2307122. https://doi.org/10.1002/advs.202307 122
- Schmid F et al. Sep., 'Calcium-binding protein S100P is a new target gene of MACC1, drives colorectal cancer metastasis and serves as a prognostic biomarker', Br. J. Cancer, 2022;127(4):675–685, https://doi.org/10.1038/s41416 -022-01833-3

#### Publisher's note

Springer Nature remains neutral with regard to jurisdictional claims in published maps and institutional affiliations.